ARTHRITIS & RHEUMATISM
Vol. 64, No. 6, June 2012, pp 1899–1908
DOI 10.1002/art.34370

Quantitative Imaging of Cartilage and Bone Morphology, Reactive Oxygen Species, and Vascularization in a Rodent Model of Osteoarthritis

LiQin Xie,[1] Angela S. P. Lin,[1] Kousik Kundu,[1] Marc E. Levenston,[2] Niren Murthy,[1] and Robert E. Guldberg[1]

Objective. **To assess temporal changes in cartilage and bone morphology, reactive oxygen species (ROS), and vascularization in rats with monosodium iodoacetate (MIA)–induced osteoarthritis (OA), using advanced imaging methodologies.**

Methods. **Right knees of 8-week-old male Wistar rats were injected with 1 mg MIA in 50 μl saline and left knees were injected with 50 μl saline as controls. After 1, 2, and 3 weeks (n = 5 at each time point), changes in cartilage morphology and composition were quantified using equilibrium partitioning of an ionic contrast agent microfocal computed tomography (μCT), and changes in subchondral and trabecular bone were assessed by standard μCT. ROS were characterized by in vivo fluorescence imaging at 1, 11, and 21 days (n = 5 at each time point). Three weeks following fluorescence imaging, alterations in knee joint vascularity were quantified with μCT after perfusion of a vascular contrast agent.**

Results. **Femoral cartilage volume, thickness, and proteoglycan content were significantly decreased in MIA-injected knees compared with control knees, accompanied by loss of trabecular bone and erosion of subchondral bone surface. ROS quantities were significantly increased 1 day after MIA injection and subsequently decreased gradually, having returned to normal by 21 days. Vascularity in whole knees and distal femora was significantly increased at 21 days after MIA injection.**

Conclusion. **Contrast-enhanced μCT and fluorescence imaging were combined to characterize articular cartilage, subchondral bone, vascularization, and ROS, providing unprecedented 3-dimensional joint imaging and quantification in multiple tissues during OA progression. These advanced imaging techniques have the potential to become standardized methods for comprehensive evaluation of articular joint degeneration and evaluation of therapeutic efficacy.**

Osteoarthritis (OA) is a highly prevalent and debilitating condition that affects multiple functionally integrated tissues within articular joints, including cartilage, subchondral bone, trabecular bone, synovium, and blood vessels (1). The pathophysiologic interactions among integrated joint tissues during initiation and progression of OA are currently poorly understood.

Subchondral bone and articular cartilage are intimately related, such that alteration in one can affect the structure and functional integrity of the other (2–4). Abnormalities in subchondral bone, such as changes in bone mineral density and bone turnover, have been suggested to contribute to the development of OA (2,5–8). Subchondral bone serves as a passive shock absorber for the joint, blunting the effects of abnormally high mechanical loads that can damage the cartilage (9). When subchondral bone becomes thicker and sclerotic, its shock-absorbing capacity decreases (9). Although the exact causes of OA are currently not fully understood, a mechanical insult to the joint is regarded as a critical extrinsic risk factor (9). Recently, studies in animal models have included longitudinal monitoring of quantitative changes in cartilage and bone (10), which can help in elucidation of the etiopathogenesis of OA and identification of effective therapies.

Supported by NIH grant R21-AR-053716.

[1]LiQin Xie, PhD, Angela S. P. Lin, MS, Kousik Kundu, PhD, Niren Murthy, PhD, Robert E. Guldberg, PhD: Georgia Institute of Technology, Atlanta; [2]Marc E. Levenston, PhD: Stanford University, Stanford, California.

Address correspondence to Robert E. Guldberg, PhD, Institute for Bioengineering and Bioscience, Georgia Institute of Technology, 315 Ferst Drive, Atlanta, GA 30332-0405. E-mail: robert.guldberg@me.gatech.edu.

Submitted for publication April 4, 2011; accepted in revised form December 27, 2011.

In contrast to the inflammatory disorder rheumatoid arthritis, OA was formerly classified as a noninflammatory disease (11). This concept has been recently revised, and it is now understood that synovial inflammation, or synovitis, plays a critical role in the symptoms and progression of OA (12). Synovial inflammation, as evidenced by stiffness, pain, and effusion, is characterized by infiltration of neutrophils, T lymphocytes, and monocytes (13) and can be assessed by magnetic resonance imaging, ultrasound, arthroscopy, and biopsy (11). The notion that synovial inflammation occurs in OA is further supported by the fact that nonsteroidal antiinflammatory drugs alleviate OA symptoms and may be more effective than simple analgesics (11,14). Synovitis can be induced by cartilage breakdown products, and its presence may increase the likelihood of meniscal and subchondral bone changes (15).

Synovial inflammation is typically accompanied by angiogenesis, and both can be triggered by the same molecular events (16). Angiogenesis is demonstrated by the growth of new blood vessels from the subchondral bone to the articular cartilage during OA progression. Inflammatory cells such as macrophages can secrete and stimulate other cells (such as endothelial cells and fibroblasts) to secrete angiogenic factors such as vascular endothelial growth factor (VEGF) (12). Angiogenesis and synovial inflammation are closely associated in OA and may contribute to the progression of cartilage degeneration and bone remodeling (17,18), in part by redistributing blood vessels (19).

The responses of individual tissues in the knee joint have been studied in the monosodium iodoacetate (MIA)–induced model of OA in the rat (20), but quantitative assessments of changes in articular cartilage, bone, vascularization, and reactive oxygen species (ROS) have not been performed together in order to determine correlations between the affected joint tissues. The objective of this study was to assess temporal changes in multiple integrated tissues of the knee joint as well as the interactions of these tissue changes during progression of disease in rats with MIA-induced OA, using advanced imaging methodologies. Changes in 3-dimensional (3-D) cartilage morphology and composition were quantified using equilibrium partitioning of an ionic contrast agent microfocal computed tomography (EPIC-μCT) imaging, changes in subchondral and trabecular bone were assessed by standard high-resolution μCT analysis, ROS during OA progression were characterized by in vivo fluorescence imaging, and alterations in the vascularity of knee joint tissues were quantified using μCT after perfusion of a vascular contrast agent.

MATERIALS AND METHODS

Assessment of cartilage and bone. The experimental procedures used in this study were approved by the Georgia Institute of Technology Institutional Animal Care and Use Committee (protocol A06005). Anesthesia was induced in 8-week-old male Wistar rats (n = 15; Charles River) by 5% isoflurane inhalation and maintained with 2% isoflurane. MIA (1 mg in 50 μl saline; Sigma-Aldrich) was injected through the infrapatellar ligament of the right knee; the left knee was injected with 50 μl saline as a control. Rats were killed via CO_2 inhalation at 1, 2, or 3 weeks after MIA injection (5 rats at each time point). The femora were harvested, dissected free of surrounding tissue, and stored in phosphate buffered saline (PBS) solution with 1% proteinase inhibitors (Cocktail I; Calbiochem) at 4°C (21).

The distal femora were prescanned for bone structure prior to incubation with contrast medium. For EPIC-μCT, the distal femur was then immersed in 2 ml of 40% Hexabrix 320 contrast agent (Covidien) and 60% PBS for 30 minutes at 37°C as described previously (21,22) and gently patted dry before scanning. Samples were scanned using a μCT 40 (Scanco Medical) at 45 kVp, 177 μA, 200 msec integration time, and a voxel size of 16 μm.

Following scanning, femora were fixed overnight in 10% neutral buffered formalin and decalcified for 10 days in 2.5% formic acid (pH 4.2). Dehydrated samples were embedded in glycol methacrylate using a JB-4 embedding kit according to the instructions of the manufacturer (Polysciences). For comparison with EPIC-μCT images, sagittal sections were cut at 8 μm thickness and 1 section through the center of each condyle was examined. Sections were stained for sulfated glycosaminoglycans (sGAGs) by sequential exposure to a 0.2% aqueous solution of fast green (1 minute), 1% glacial acetic acid in 70% ethanol (10 seconds), deionized water (1 minute), and 0.5% Safranin O in distilled water (5 minutes).

In vivo quantification of ROS. Eight-week-old male Wistar rats (n = 5) were anesthetized by isoflurane inhalation, and 1 mg of MIA in 50 μl saline was injected through the infrapatellar ligament of the right knee, with the left knee injected with saline as a control. On day 1, day 11, or day 21 after injection of MIA solution, rats were anesthetized by isoflurane inhalation, and 1 mg hydro–indocyanine green (hydro-ICG) in 50 μl saline was injected intraarticularly into both knees to image ROS production. Immediately following injection, rats were allowed to recover from anesthesia and ambulate freely in their cages. A 10-day interval between sequential injections was chosen to ensure clearance of the hydro-ICG probe from the joint and return of fluorescence intensity to the baseline level. One hour after injection of the hydro-ICG solution, rats were anesthetized with isoflurane, and in vivo fluorescence images were captured using a Xenogen IVIS Lumina system (Caliper). The excitation and emission wavelengths for hydro-ICG were 745 nm and 840 nm, respectively, and the exposure time was 12 seconds.

Assessment of vascularity. Three weeks after MIA injection, the rats that were used for ROS imaging were anesthetized with isoflurane, isoflurane was maintained at the

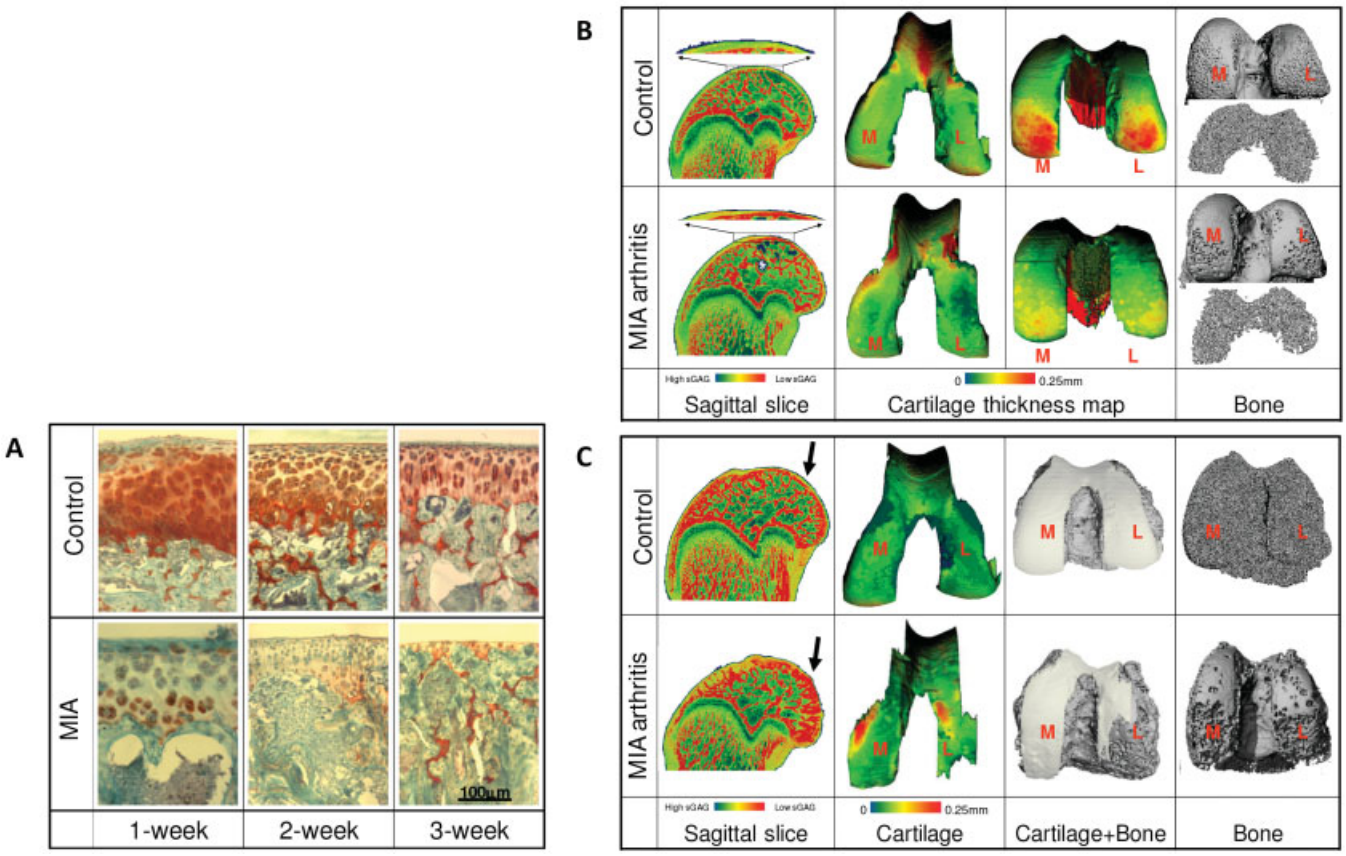

Figure 1. A, Representative Safranin O–stained sagittal sections of femoral articular cartilage obtained from the knees of rats 1, 2, or 3 weeks after injection of monosodium iodoacetate (MIA) to induce osteoarthritis and injection of saline into the contralateral knee as a control. **B** and **C,** Equilibrium partitioning of an ionic contrast agent microfocal computed tomography (μCT) images of cartilage x-ray attenuation (sagittal slices), cartilage thickness maps, and standard μCT images of subchondral and trabecular bone in distal femora at 1 week (**B**) and 3 weeks (**C**) after injection of MIA or saline. **Arrows** in **C** indicate a region of denuded subchondral bone with no cartilage coverage in the MIA-injected femoral condyle, in contrast to a healthy cartilage layer in the control. M = medial; L = lateral; sGAG = sulfated glycosaminoglycan.

induction-level dose, and the vascular systems of the rats were sequentially perfused with 0.9% physiologic saline solution, 10% neutral buffered formalin, and a lead chromate–based contrast agent (Microfil MV-122; FlowTech) via a needle passed through the left ventricle and into the aorta. This technique was slightly modified from a previously published methodology for contrast-enhanced imaging of vascular structures (23). After polymerization overnight, both knee joints were dissected to remove the attached muscles and were scanned by μCT at 45 kVp, 177 μA, 200 msec integration time, and a voxel size of 16 μm. Following demineralization for 10 days with 10% formic acid, both knee joints and dissected femora were scanned (voxel size 16 μm and 10 μm, respectively).

Statistical analysis. Data were expressed as the mean ± SD. Cartilage and bone morphologic parameters and fluorescence intensities at different time points after MIA injection were evaluated using a one-factor (time) repeated (left versus right) generalized linear model with Tukey's test for post hoc analysis. Differences in vascularization between control and MIA-injected knees were compared by paired *t*-test. *P* values less than or equal to 0.05 were considered significant. Statistical calculations were performed with SPSS, version 11.

RESULTS

Representative images of femoral articular cartilage sections stained with Safranin O are shown in Figure 1A. At 1 week postinjection, the thickness and sGAG optical density of cartilage from rats injected with MIA were decreased compared with control cartilage from the contralateral femora. At 2 and 3 weeks postinjection, part of the subchondral bone surface was denuded without cartilage coverage, especially in load-bearing regions of the condyles of MIA-treated animals.

Figures 1B and C show representative images of

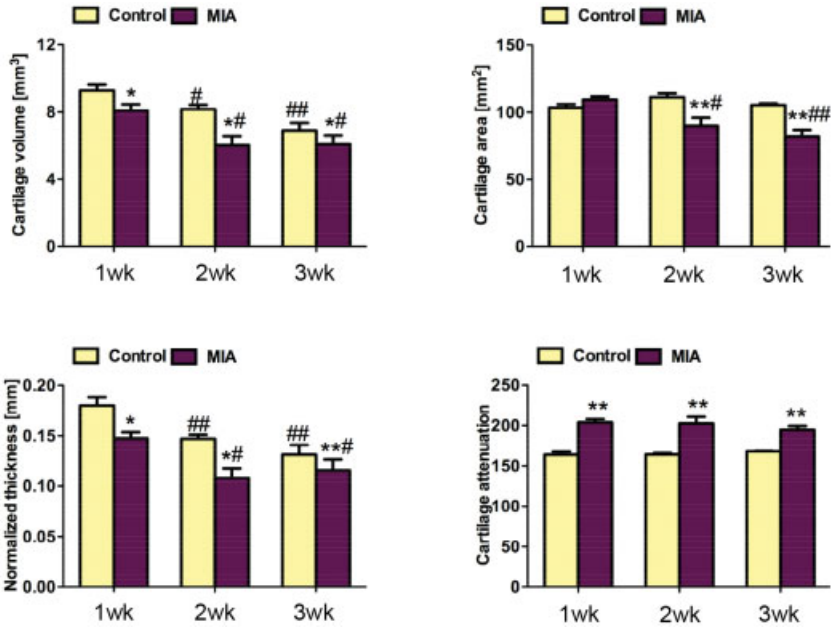

Figure 2. Quantification of cartilage properties in the distal femoral condyles of control and monosodium iodoacetate (MIA)–injected knees at 1, 2, and 3 weeks postinjection. Cartilage volume, area, normalized thickness, and attenuation were measured. At 1 week postinjection, cartilage volume and normalized thickness (volume/bone surface interface area) were significantly lower in MIA-injected joints than in contralateral saline-injected joints (controls). At 2 weeks and 3 weeks postinjection, cartilage volume, area, and normalized thickness were significantly lower in MIA-injected joints than in control joints. Average cartilage attenuation was significantly higher in MIA-injected joints than in control joints at all time points. Values are the mean ± SD. $* = P < 0.05$; $** = P < 0.01$ versus control. $\# = P < 0.05$; $\#\# = P < 0.01$ versus 1 week postinjection. Color figure can be viewed in the online issue, which is available at http://onlinelibrary.wiley.com/journal/10.1002/(ISSN)1529-0131.

3-D morphology of rat femoral articular cartilage and bone. Consistent with our previous studies (22,24), we were able to segment cartilage from bone and therefore analyze cartilage in the 3-D EPIC-μCT images. At 1 week after injection, volume and normalized thickness (volume/bone surface interface area) of cartilage from MIA-injected joints were 13% and 18% lower, respectively, than in contralateral control cartilage ($P < 0.05$), while cartilage attenuation was 24% higher than in control cartilage ($P < 0.01$) (Figures 1B and 2). This suggested that sGAG content was lower in the femoral articular cartilage of MIA-treated animals (22,24). Trabecular bone volume fraction (bone volume/trabecular volume [BV/TV]) and trabecular thickness (TbTh) in the femoral epiphyses of MIA-treated rats were 17% and 10% lower, respectively, than in controls ($P < 0.05$ and $P < 0.01$, respectively) (Figures 1B and 3).

At 2 weeks postinjection, femoral articular cartilage volume, area, and normalized thickness were lower in MIA-injected joints than in controls by 26% ($P < 0.05$), 19% ($P < 0.01$), and 26% ($P < 0.05$), respectively, and attenuation was 24% higher than in controls ($P < 0.01$) (Figure 2). An average of 12% of the surface was denuded subchondral bone with no cartilage coverage. BV/TV, connectivity density (ConnD), and TbTh in the femoral epiphyses were 22%, 26%, and 7% lower, respectively, than in controls (all $P < 0.01$) (Figure 3).

At 3 weeks after injection, femoral articular cartilage volume, area, and normalized thickness in MIA-injected joints were 12%, 22%, and 12% lower, respectively, than in controls ($P < 0.05$, $P < 0.01$, and $P < 0.01$, respectively), while attenuation was 16% higher than in controls ($P < 0.01$) (Figures 1C and 2). An average of 14% of the surface was denuded bone without cartilage coverage. BV/TV, ConnD, and trabecular number in the femoral epiphysis were 20%, 20%, and 6% lower, respectively, in MIA-injected joints than in controls ($P < 0.01$, $P < 0.05$, and $P < 0.05$, respectively) (Figure 3).

Within joints (control or MIA injected), morphologic changes in femoral articular cartilage were seen over time, but compositional changes were not. Femoral cartilage volume and normalized thickness were significantly lower both in control and in MIA-injected joints at 2 weeks and 3 weeks postinjection compared with 1 week postinjection (in MIA-injected joints, $P < 0.05$ for

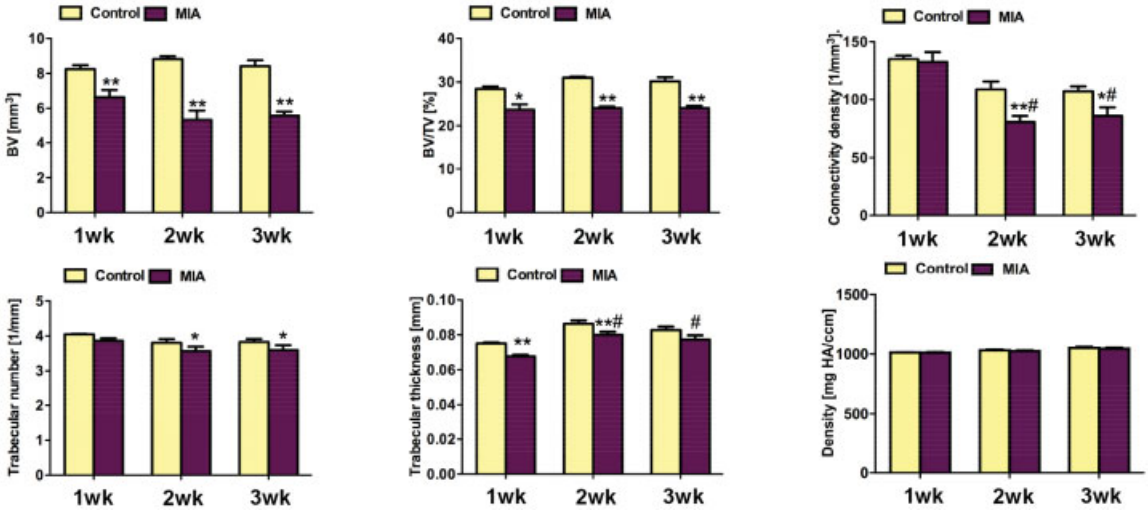

Figure 3. Quantification of trabecular bone morphometry in the distal femoral epiphyses of control and monosodium iodoacetate (MIA)–injected knees at 1, 2, and 3 weeks postinjection. Bone volume (BV), bone volume/total volume (BV/TV), connectivity density (ConnD), trabecular number (TbN), trabecular thickness (TbTh), and bone mineral density (assessed as milligrams hydroxyapatite [HA] per cubic centimeter) were measured. At 1 week postinjection, BV, BV/TV and TbTh were significantly lower in the MIA-treated femoral epiphyses than in the contralateral control epiphyses. At 2 weeks postinjection, BV, BV/TV, ConnD, TbN, and TbTh were significantly lower in the MIA-treated femoral epiphyses than in control epiphyses. At 3 weeks postinjection, BV, BV/TV, ConnD, and TbN were significantly lower in the MIA-treated femoral epiphyses than in control epiphyses. Average bone mineral density in the femoral epiphysis was not significantly different between MIA-treated and control epiphyses at any of the 3 time points. Values are the mean ± SD. $* = P < 0.05$; $** = P < 0.01$ versus control. $\# = P < 0.05$ versus 1 week postinjection. Color figure can be viewed in the online issue, which is available at http://onlinelibrary.wiley.com/journal/10.1002/(ISSN)1529-0131.

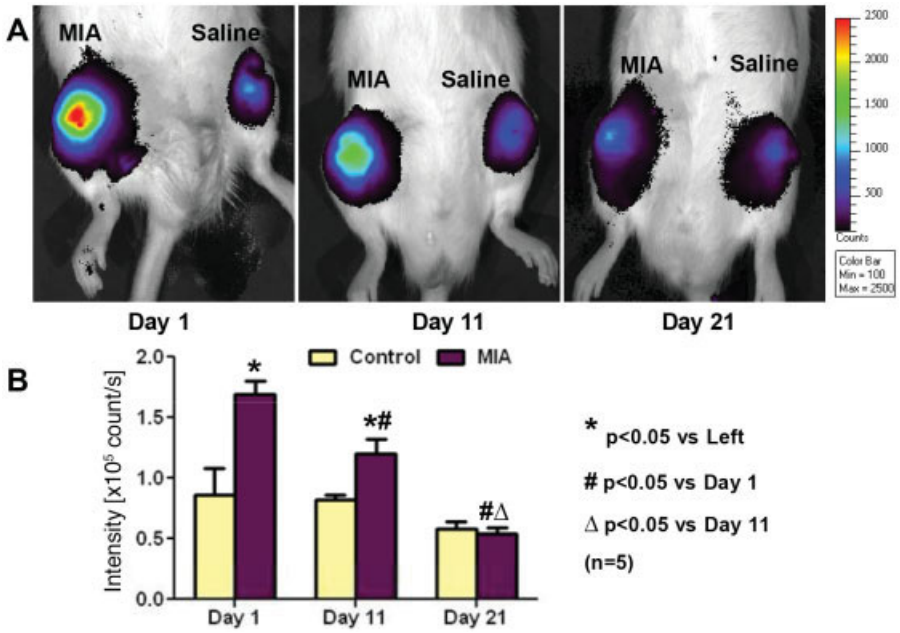

Figure 4. Fluorescence imaging of reactive oxygen species (ROS) as an indicator of inflammatory response in rat joints with monosodium iodoacetate (MIA)–induced osteoarthritis and contralateral control saline-injected joints. **A,** Hydro–indocyanine green ROS images were obtained 1, 11, and 21 days postinjection. A representative image from each time point is shown. **B,** Fluorescence intensity was significantly higher in MIA-injected joints than in control joints 1 day and 11 days postinjection, but there was no difference at 21 days. Fluorescence intensity decreased significantly over time in MIA-injected joints, but not in control joints. Values are the mean ± SD. Color figure can be viewed in the online issue, which is available at http://onlinelibrary.wiley.com/journal/10.1002/(ISSN)1529-0131.

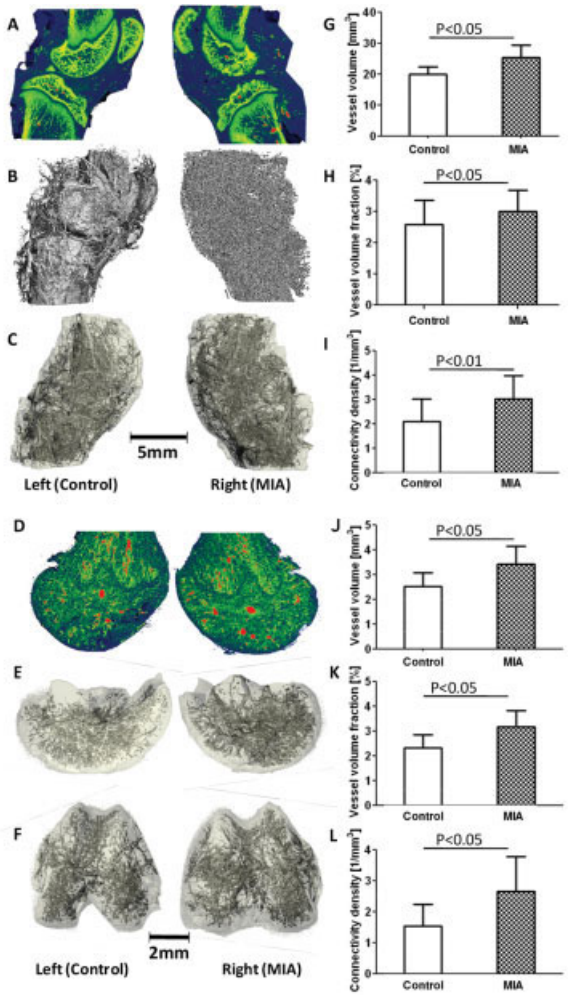

Figure 5. Assessment of vascularization 3 weeks after injection of monosodium iodoacetate (MIA) into the knee joints of rats to induce osteoarthritis and injection of saline into the contralateral knee as a control. **A,** Representative sagittal section x-ray attenuation maps of MIA-injected and control joints, including bone and vasculature. Red indicates the higher-attenuating contrast-perfused vasculature; green/yellow indicates bone. **B,** Segmented microfocal tomography (μCT) images of the whole joints, including both bone and vasculature. **C,** Postdecalcification images depicting the full 3-dimensional (3-D) vascular network within and surrounding the joints. **D,** Sagittal section x-ray attenuation maps of the decalcified distal femora. Red indicates higher-attenuating main vasculature; green indicates the smaller surrounding vessels. **E,** Segmented 3-D μCT image of vasculature within the distal femora (lateral view). **F,** Segmented 3-D μCT image of vasculature within the distal femora (distal condylar view). **G–I,** Quantitative findings in whole joints, showing significant increases in vascular volume (**G**), vascular volume fraction (**H**), and connectivity density (**I**) in MIA-injected joints versus control joints 3 weeks after injection. **J–L,** Quantitative findings in isolated distal femora, showing results similar to those obtained for the whole joint, i.e., significant increases in vascular volume (**J**), vascular volume fraction (**K**), and connectivity density (**L**). Values in **G–L** are the mean ± SD. Color figure can be viewed in the online issue, which is available at http://onlinelibrary.wiley.com/journal/10.1002/(ISSN)1529-0131.

cartilage volume and normalized thickness at 2 weeks and 3 weeks; in control joints, $P < 0.05$ for cartilage volume at 2 weeks, and $P < 0.01$ for cartilage volume at 3 weeks and for normalized thickness at 2 weeks and 3 weeks) (Figure 2). There was no significant difference in femoral cartilage attenuation among the 3 time points in either control or MIA-injected joints (Figure 2D). With MIA injection, ConnD for trabecular bone in the femoral epiphysis was lower ($P < 0.05$), while TbTh was higher ($P < 0.05$), at 2 weeks and 3 weeks compared with 1 week after injection (Figure 3).

Representative fluorescence hydro-ICG ROS images (Figure 4A) demonstrated that ROS quantities were increased in the knees of rats with MIA-induced OA, and this effect lessened with increased time after MIA injection. The fluorescence intensity was 98% higher in the MIA-injected joints than in the control joints (n = 5 per group) at 1 day after injection (mean ± SD $1.69 \pm 0.25 \times 10^5$ counts/second versus $0.86 \pm 0.51 \times 10^5$ counts/second; $P < 0.05$) and 46% higher at 11 days after injection ($1.20 \pm 0.27 \times 10^5$ counts/second versus $0.82 \pm 0.09 \times 10^5$ counts/second; $P < 0.05$) (Figure 4B). However, by 21 days after injection, fluorescence intensity was no longer significantly different between the 2 groups ($0.54 \pm 0.12 \times 10^5$ counts/second versus $0.58 \pm 0.13 \times 10^5$ counts/second in the MIA and control groups, respectively). Within the group of control-injected knees, fluorescence intensity did not change significantly during the 21-day period after injection. However, within the group of MIA-injected joints, fluorescence intensity decreased by 29% from day 1 to day 11 after injection ($P < 0.05$) and further decreased by 54% from day 11 to day 21 ($P < 0.05$), reaching the level observed in control knees (Figure 4B).

Three weeks after injection of MIA to induce OA, vascularization in both knee joints and distal femora was assessed. Sagittal attenuation maps demonstrated erosions on the subchondral bone surfaces of the patella, femur, and tibia in the OA knee joints (Figure 5A). The main blood vessels perfused with contrast agent had higher attenuation than the surrounding bone tissue. The 3-D vascular network surrounding the knee joint, including all combined capsule, subchondral and trabecular bone, synovium, and meniscal tissues, is shown in Figure 5B. In the decalcified vascularity maps shown in Figure 5C, the 3-D vascular distribution in the whole knee joint is demonstrated more clearly because mineral has been cleared and surrounding tissues are depicted transparently. Vessel volume, vessel volume fraction, and vessel connectivity density were 27% ($P < 0.05$), 16% ($P < 0.05$), and 44% ($P < 0.01$) higher,

respectively, in the MIA-injected OA knee joints than in the contralateral control joints (Figures 5G–I). Attenuation maps of sagittal sections of the decalcified distal femur are shown in Figure 5D. Segmented images of the vasculature with surrounding tissues depicted transparently are shown in Figures 5E and F. Quantitative results were similar to results from the whole knee joint. Vessel volume, vessel volume fraction, and vessel connectivity density were 34%, 30%, and 60% higher, respectively, in the OA distal femora than in the control femora (all $P < 0.05$) (Figures 5J–L).

DISCUSSION

Current techniques for evaluation of OA in animal models, such as histologic scoring and biochemical assays, require specimen destruction, are time consuming, and cannot be used to assess the 3-D spatial morphology of articular cartilage and blood vessels. Cartilage histologic scoring methods require scoring of ~10 sections across the whole knee joint, and the semiquantitative scores are subjective, with intra- and interobserver variation (25,26). Three-dimensional morphometric analysis of images by μCT offers distinct advantages compared with 2-D histomorphometry, e.g., eliminating the need for exact specimen positioning and alignment (27), eliminating possible artifacts caused by sample fixation, dehydration, embedding, and sectioning (28), and providing more precise thickness measurements via sphere fitting and more complete quantitative volumetric assessments (29,30). Following nondestructive μCT scanning with Hexabrix or Microfil contrast agents, most standard histologic processes (e.g., Safranin O staining in this study) can still be performed.

Microfocal CT enables 3-D quantitative morphologic analysis of hard tissues at micron-level voxel resolutions and has been used to monitor progressive changes in the subchondral bone of rats injected with MIA (31). As MIA-induced OA is not a surgically induced mechanical instability model of the disease, joints were not expected to exhibit subchondral sclerosis or thickening of the subchondral bone plate, which has been observed in guinea pigs with spontaneous OA (32), rabbits with meniscectomy-induced OA (33), rats with anterior cruciate ligament transection (7), mice with spontaneous OA (34), and human OA patients (35,36). Previous studies have demonstrated thinner trabeculae in mice with MIA- or collagenase-induced OA (37,38). However, it was still surprising that only 1 week postinjection, there were significant decreases in trabecular bone volume fraction and trabecular thickness in femoral epiphyses. The exact mechanism of the decrease in trabeculae is unknown, but potential causes may be skeletal disuse, inflammation, ROS, and activation of osteoclasts (37). It has been shown that locomotor activity significantly decreases after MIA injection (20) due to the severe pain induced by inflammation in the MIA-injected OA knee joint (39). Accordingly, our results suggest that the change in trabecular volume fraction could provide a sensitive and quantitative index of disuse and pain.

Our previous studies indicated that EPIC-μCT imaging enables nondestructive assessment of cartilage morphology and composition in rat articular cartilage, with high precision and accuracy (22,24). In the present study, we were able to use EPIC-μCT to quantitatively depict the temporal changes in 3-D cartilage morphology and composition in the rat distal femora in an MIA-induced OA model. MIA inhibits the activity of G3PDH in chondrocytes, resulting in disruption of glycolysis and eventually, cell death (39). Destructive enzymatic activity causes proteoglycan degradation, chondrocyte necrobiosis, and disruption of the collagen network, resulting in progressive impairment of mechanical function (40–43). This interaction between biochemical and mechanical factors created a progressive cycle of cartilage degradation and subchondral bone loss. The decreases in cartilage volume, area, thickness, and sGAG content were accompanied by loss of trabecular bone and erosion of subchondral bone surface in the distal femora, and these changes detected by μCT corresponded to the results of histologic evaluation. The ability to combine standard μCT and EPIC-μCT to quantitatively analyze cartilage and bone from the same joint provided improved understanding of the interactions between cartilage and bone during the progression of OA.

Reactive oxygen species (superoxide and the hydroxyl radical) are toxic and could play an important role in the initiation and pathophysiology of OA (44). Currently used fluorescent probes, such as dihydroethidium, have several problems that limit their wider application. Our group has developed a novel class of fluorescent sensors, hydrocyanines, that can be used to image ROS in vivo (45,46). Hydrocyanines have nanomolar sensitivity toward the hydroxyl radical with a linear response and are significantly more sensitive than the previous dihydroethidium probes. Using this technique in the present study, the fluorescence intensity we observed in knees with MIA-induced OA indicated that

high levels of ROS were present in the synovial capsule 1 day after MIA injection and were gradually relieved by 21 days. This study demonstrates that in vivo fluorescence imaging can be used to noninvasively quantify ROS during OA progression and to assess the efficacy of pharmacologic interventions in small animals. Additionally, the use of hydrocyanines to image ROS has the potential to be a powerful clinical tool in diagnosing OA and monitoring treatment efficacy in humans.

Demonstration of the perfusion of a radiodense contrast agent into blood vessels has allowed indirect nondestructive imaging of 3-D vascularity such that vascular volume, vessel thickness, and connectivity density can be quantified postmortem (47–50). In this study we have shown that μCT with contrast agent perfusion could be utilized to quantify 3-D vascularity in a small animal OA model, providing evidence, for the first time, of higher vascularity in OA-affected whole knee joints and distal femora. These findings suggest the importance of angiogenesis in the progression of OA, consistent with results showing that vascular invasion into subchondral bone contributes to cartilage degradation by inducing expression of matrix metalloproteinases in OA (51). Although the exact mechanisms of angiogenesis in OA are still not clear, the high levels of ROS and early synovial inflammation indicated by joint swelling on day 1 postinjection are thought to play an important role in this pathologic regeneration (16). ROS can induce VEGF expression (52), which may stimulate angiogenesis, and increased VEGF expression has been detected as early as 1 week after surgery in the rat OA model (12,53). The combination of angiogenesis and ROS might also exacerbate the progression of cartilage degeneration and bone remodeling (17,18,54).

Providing a methodology that enables the creation of 3-D articular cartilage thickness and topography maps may impact many relevant applications. Using high-resolution 3-D cartilage thickness maps, focal variations in cartilage thickness can be visualized with a color scale, and the cartilage contact area and surface stresses can be estimated (29,55). Thickness and topography maps can also be used to evaluate joint mechanics and mechanoadaptation of articular cartilage (56). In addition, these maps could be utilized to define the relationship between genetic background and cartilage phenotype (37) and to provide guidance in the design of prosthetic surfaces and tissue engineering constructs.

The MIA OA model is minimally invasive, reproducibly induces OA-like lesions, and has been widely used in OA animal studies (20,31,57,58). One of the limitations of the present study was the use of saline-injected contralateral limbs as controls rather than using naive, age-matched control animals. The mobility of mice with MIA decreased while loading of the contralateral limbs increased compared with the MIA-injected limbs (20), suggesting that the contralateral limb may not be truly normal. In this study, histologic analysis of the contralateral femora showed no apparent pathologic changes in bone or cartilage, supporting the use of contralateral limbs as an internal control. Nevertheless, inclusion of age-matched control animals could provide additional insights into specific effects of MIA. MIA-induced arthritis is an aggressive model of cartilage degeneration and subchondral bone remodeling and is suitable for evaluating ROS, inflammation, pain, and angiogenesis during OA progression. However, the aggressiveness of this model limited our ability to elaborate on the relationship between cartilage degeneration and subchondral bone remodeling during early OA initiation in the present study. Further research is needed to study multiple tissues via these novel techniques in the setting of more gradually progressive disease, e.g., spontaneous or surgically induced OA, which are more similar to early OA in humans.

In summary, this is the first study to quantify the temporal changes in articular cartilage, subchondral bone, ROS, and vascularization via fluorescence imaging and contrast-enhanced μCT in a rat model of MIA-induced OA. The ability to quantitatively evaluate changes in multiple tissues during the initiation and progression of OA may improve our understanding of the interactive changes in multiple tissues in OA pathophysiology and provide insights for development of new treatment modalities. These advanced imaging techniques have the potential to become standardized analysis methods for comprehensive evaluation of articular joint degeneration and treatment efficacy.

AUTHOR CONTRIBUTIONS

All authors were involved in drafting the article or revising it critically for important intellectual content, and all authors approved the final version to be published. Dr. Guldberg had full access to all of the data in the study and takes responsibility for the integrity of the data and the accuracy of the data analysis.

Study conception and design. Xie, Lin, Levenston, Murthy, Guldberg.
Acquisition of data. Xie, Lin, Kundu.
Analysis and interpretation of data. Xie, Lin, Levenston, Murthy, Guldberg.

REFERENCES

1. Goldring MB, Goldring SR. Articular cartilage and subchondral bone in the pathogenesis of osteoarthritis. Ann N Y Acad Sci 2010;1192:230–7.

2. Blair-Levy JM, Watts CE, Fiorentino NM, Dimitriadis EK, Marini JC, Lipsky PE. A type I collagen defect leads to rapidly progressive osteoarthritis in a mouse model. Arthritis Rheum 2008;58: 1096–106.
3. Mrosek EH, Lahm A, Erggelet C, Uhl M, Kurz H, Eissner B, et al. Subchondral bone trauma causes cartilage matrix degeneration: an immunohistochemical analysis in a canine model. Osteoarthritis Cartilage 2006;14:171–8.
4. Radin EL, Rose RM. Role of subchondral bone in the initiation and progression of cartilage damage. Clin Orthop Relat Res 1986;213:34–40.
5. Lajeunesse D, Reboul P. Subchondral bone in osteoarthritis: a biologic link with articular cartilage leading to abnormal remodeling. Curr Opin Rheumatol 2003;15:628–33.
6. Antoniades L, MacGregor AJ, Matson M, Spector TD. A cotwin control study of the relationship between hip osteoarthritis and bone mineral density. Arthritis Rheum 2000;43:1450–5.
7. Hayami T, Pickarski M, Zhuo Y, Wesolowski GA, Rodan GA, le Duong T. Characterization of articular cartilage and subchondral bone changes in the rat anterior cruciate ligament transection and meniscectomized models of osteoarthritis. Bone 2006;38:234–43.
8. Bettica P, Cline G, Hart DJ, Meyer J, Spector TD. Evidence for increased bone resorption in patients with progressive knee osteoarthritis: longitudinal results from the Chingford study. Arthritis Rheum 2002;46:3178–84.
9. Brandt KD, Dieppe P, Radin E. Etiopathogenesis of osteoarthritis. Med Clin North Am 2009;93:1–24, xv.
10. Calvo E, Palacios I, Delgado E, Sanchez-Pernaute O, Largo R, Egido J, et al. Histopathological correlation of cartilage swelling detected by magnetic resonance imaging in early experimental osteoarthritis. Osteoarthritis Cartilage 2004;12:878–86.
11. Ashraf S, Walsh DA. Angiogenesis in osteoarthritis. Curr Opin Rheumatol 2008;20:573–80.
12. Bonnet CS, Walsh DA. Osteoarthritis, angiogenesis and inflammation. Rheumatology (Oxford) 2005;44:7–16.
13. Sutton S, Clutterbuck A, Harris P, Gent T, Freeman S, Foster N, et al. The contribution of the synovium, synovial derived inflammatory cytokines and neuropeptides to the pathogenesis of osteoarthritis. Vet J 2009;179:10–24.
14. Case JP, Baliunas AJ, Block JA. Lack of efficacy of acetaminophen in treating symptomatic knee osteoarthritis: a randomized, double-blind, placebo-controlled comparison trial with diclofenac sodium. Arch Intern Med 2003;163:169–78.
15. Hellio Le Graverand-Gastineau MP. OA clinical trials: current targets and trials for OA. Choosing molecular targets: what have we learned and where we are headed? Osteoarthritis Cartilage 2009;17:1393–401.
16. Costa C, Incio J, Soares R. Angiogenesis and chronic inflammation: cause or consequence? Angiogenesis 2007;10:149–66.
17. Imhof H, Breitenseher M, Kainberger F, Trattnig S. Degenerative joint disease: cartilage or vascular disease? Skeletal Radiol 1997; 26:398–403.
18. Haywood L, McWilliams DF, Pearson CI, Gill SE, Ganesan A, Wilson D, et al. Inflammation and angiogenesis in osteoarthritis. Arthritis Rheum 2003;48:2173–7.
19. Mapp PI, Avery PS, McWilliams DF, Bowyer J, Day C, Moores S, et al. Angiogenesis in two animal models of osteoarthritis. Osteoarthritis Cartilage 2008;16:61–9.
20. Guingamp C, Gegout-Pottie P, Philippe L, Terlain B, Netter P, Gillet P. Mono-iodoacetate–induced experimental osteoarthritis: a dose–response study of loss of mobility, morphology, and biochemistry. Arthritis Rheum 1997;40:1670–9.
21. Palmer AW, Guldberg RE, Levenston ME. Analysis of cartilage matrix fixed charge density and three-dimensional morphology via contrast-enhanced microcomputed tomography. Proc Natl Acad Sci U S A 2006;103:19255–60.
22. Xie L, Lin AS, Levenston ME, Guldberg RE. Quantitative assessment of articular cartilage morphology via EPIC-microCT. Osteoarthritis Cartilage 2009;17:313–20.
23. Duvall CL, Taylor WR, Weiss D, Guldberg RE. Quantitative microcomputed tomography analysis of collateral vessel development after ischemic injury. Am J Physiol Heart Circ Physiol 2004;287:H302–10.
24. Xie L, Lin AS, Guldberg RE, Levenston ME. Nondestructive assessment of sGAG content and distribution in normal and degraded rat articular cartilage via EPIC-microCT. Osteoarthritis Cartilage 2010;18:65–72.
25. Gerwin N, Bendele AM, Glasson S, Carlson CS. The OARSI histopathology initiative: recommendations for histological assessments of osteoarthritis in the rat. Osteoarthritis Cartilage 2010;18 Suppl 3:S24–34.
26. Glasson SS, Chambers MG, van den Berg WB, Little CB. The OARSI histopathology initiative: recommendations for histological assessments of osteoarthritis in the mouse. Osteoarthritis Cartilage 2010;18 Suppl 3:S17–23.
27. Xia Y. The total volume and the complete thickness of articular cartilage determined by MRI. Osteoarthritis Cartilage 2003;11: 473–4.
28. Uchiyama T, Tanizawa T, Muramatsu H, Endo N, Takahashi HE, Hara T. A morphometric comparison of trabecular structure of human ilium between microcomputed tomography and conventional histomorphometry. Calcif Tissue Int 1997;61:493–8.
29. Millington SA, Grabner M, Wozelka R, Anderson DD, Hurwitz SR, Crandall JR. Quantification of ankle articular cartilage topography and thickness using a high resolution stereophotography system. Osteoarthritis Cartilage 2007;15:205–11.
30. Laib A, Barou O, Vico L, Lafage-Proust MH, Alexandre C, Rugsegger P. 3D micro-computed tomography of trabecular and cortical bone architecture with application to a rat model of immobilisation osteoporosis. Med Biol Eng Comput 2000;38: 326–32.
31. Morenko BJ, Bove SE, Chen L, Guzman RE, Juneau P, Bocan TM, et al. In vivo micro computed tomography of subchondral bone in the rat after intra-articular administration of monosodium iodoacetate. Contemp Top Lab Anim Sci 2004;43:39–43.
32. Anderson-MacKenzie JM, Quasnichka HL, Starr RL, Lewis EJ, Billingham ME, Bailey AJ. Fundamental subchondral bone changes in spontaneous knee osteoarthritis. Int J Biochem Cell Biol 2005;37:224–36.
33. Fahlgren A, Messner K, Aspenberg P. Meniscectomy leads to an early increase in subchondral bone plate thickness in the rabbit knee. Acta Orthop Scand 2003;74:437–41.
34. Wachsmuth L, Engelke K. High-resolution imaging of osteoarthritis using microcomputed tomography. Methods Mol Med 2004; 101:231–48.
35. Ding M, Odgaard A, Hvid I. Changes in the three-dimensional microstructure of human tibial cancellous bone in early osteoarthritis. J Bone Joint Surg Br 2003;85:906–12.
36. Hochberg MC, Lethbridge-Cejku M, Tobin JD. Bone mineral density and osteoarthritis: data from the Baltimore Longitudinal Study of Aging. Osteoarthritis Cartilage 2004;12 Suppl A:S45–8.
37. Botter SM, van Osch GJ, Waarsing JH, van der Linden JC, Verhaar JA, Pols HA, et al. Cartilage damage pattern in relation to subchondral plate thickness in a collagenase-induced model of osteoarthritis. Osteoarthritis Cartilage 2008;16:506–14.
38. Koh YH, Hong SH, Kang HS, Chung CY, Koo KH, Chung HW, et al. The effects of bone turnover rate on subchondral trabecular bone structure and cartilage damage in the osteoarthritis rat model. Rheumatol Int 2010;30:1165–71.
39. Beyreuther B, Callizot N, Stohr T. Antinociceptive efficacy of lacosamide in the monosodium iodoacetate rat model for osteoarthritis pain. Arthritis Res Ther 2007;9:R14.
40. Armstrong CG, Mow VC. Variations in the intrinsic mechanical

properties of human articular cartilage with age, degeneration, and water content. J Bone Joint Surg Am 1982;64:88–94.
41. Williamson AK, Chen AC, Sah RL. Compressive properties and function-composition relationships of developing bovine articular cartilage. J Orthop Res 2001;19:1113–21.
42. Rieppo J, Toyras J, Nieminen MT, Kovanen V, Hyttinen MM, Korhonen RK, et al. Structure-function relationships in enzymatically modified articular cartilage. Cells Tissues Organs 2003;175: 121–32.
43. LeRoux MA, Arokoski J, Vail TP, Guilak F, Hyttinen MM, Kiviranta I, et al. Simultaneous changes in the mechanical properties, quantitative collagen organization, and proteoglycan concentration of articular cartilage following canine meniscectomy. J Orthop Res 2000;18:383–92.
44. Regan E, Flannelly J, Bowler R, Tran K, Nicks M, Carbone BD, et al. Extracellular superoxide dismutase and oxidant damage in osteoarthritis. Arthritis Rheum 2005;52:3479–91.
45. Kundu K, Knight SF, Willett N, Lee S, Taylor WR, Murthy N. Hydrocyanines: a class of fluorescent sensors that can image reactive oxygen species in cell culture, tissue, and in vivo. Angew Chem Int Ed Engl 2009;48:299–303.
46. Lee D, Khaja S, Velasquez-Castano JC, Dasari M, Sun C, Petros J, et al. In vivo imaging of hydrogen peroxide with chemiluminescent nanoparticles. Nat Mater 2007;6:765–9.
47. Garcia-Sanz A, Rodriguez-Barbero A, Bentley MD, Ritman EL, Romero JC. Three-dimensional microcomputed tomography of renal vasculature in rats. Hypertension 1998;31:440–4.
48. Jorgensen SM, Demirkaya O, Ritman EL. Three-dimensional imaging of vasculature and parenchyma in intact rodent organs with X-ray micro-CT. Am J Physiol 1998;275:H1103–14.
49. Paulus MJ, Gleason SS, Kennel SJ, Hunsicker PR, Johnson DK. High resolution X-ray computed tomography: an emerging tool for small animal cancer research. Neoplasia 2000;2:62–70.
50. Bentley MD, Ortiz MC, Ritman EL, Romero JC. The use of microcomputed tomography to study microvasculature in small rodents. Am J Physiol Regul Integr Comp Physiol 2002;282: R1267–79.
51. Shibakawa A, Yudoh K, Masuko-Hongo K, Kato T, Nishioka K, Nakamura H. The role of subchondral bone resorption pits in osteoarthritis: MMP production by cells derived from bone marrow. Osteoarthritis Cartilage 2005;13:679–87.
52. Fay J, Varoga D, Wruck CJ, Kurz B, Goldring MB, Pufe T. Reactive oxygen species induce expression of vascular endothelial growth factor in chondrocytes and human articular cartilage explants. Arthritis Res Ther 2006;8:R189.
53. Hayami T, Funaki H, Yaoeda K, Mitui K, Yamagiwa H, Tokunaga K, et al. Expression of the cartilage derived anti-angiogenic factor chondromodulin-I decreases in the early stage of experimental osteoarthritis. J Rheumatol 2003;30:2207–17.
54. Henrotin Y, Kurz B, Aigner T. Oxygen and reactive oxygen species in cartilage degradation: friends or foes? Osteoarthritis Cartilage 2005;13:643–54.
55. Koo S, Gold GE, Andriacchi TP. Considerations in measuring cartilage thickness using MRI: factors influencing reproducibility and accuracy. Osteoarthritis Cartilage 2005;13:782–9.
56. Eckstein F, Reiser M, Englmeier KH, Putz R. In vivo morphometry and functional analysis of human articular cartilage with quantitative magnetic resonance imaging: from image to data, from data to theory. Anat Embryol (Berl) 2001;203:147–73.
57. Guzman RE, Evans MG, Bove S, Morenko B, Kilgore K. Monoiodoacetate-induced histologic changes in subchondral bone and articular cartilage of rat femorotibial joints: an animal model of osteoarthritis. Toxicol Pathol 2003;31:619–24.
58. Piscaer TM, Waarsing JH, Kops N, Pavljasevic P, Verhaar JA, van Osch GJ, et al. In vivo imaging of cartilage degeneration using microCT-arthrography. Osteoarthritis Cartilage 2008;16:1011–7.